Hindawi
Journal of Nanomaterials
Volume 2022, Article ID 6822884, 20 pages
https://doi.org/10.1155/2022/6822884

Research Article

Analyzing Characteristics for Two-Step SET Operation Scheme for Improving Write Time in Nanoscale Phase-Change Memory (PCM)

Milad Mohseni,[1] **Ahmed Alkhayyat**,[2] **P. Balaji Srikaanth**,[3] **Ali Jawad Alrubaie**,[4] **Arnold C. Alguno**,[5] **Rey Y. Capangpangan**,[6] **and Bhupesh Kumar Singh**[7]

[1]*Department of Computer Engineering, Islamic Azad University, Tabriz, Iran*
[2]*Department of Computer Technical Engineering, College of Technical Engineering, Najaf, Iraq*
[3]*Department of Networking and Communications, School of Computing, SRM Institute of Science and Technology Kattankulathur Campus, Chennai, India*
[4]*Department of Medical Instrumentation Techniques Engineering, Al-Mustaqbal University College, Babylon, Iraq*
[5]*Department of Physics, Mindanao State University-Iligan Institute of Technology, Tibanga Highway, Iligan City 9200, Philippines*
[6]*Department of Physical Sciences and Mathematics, College of Science and Environment Mindanao State University at Naawan, Naawan, Misamis Oriental 9023, Philippines*
[7]*Arba Minch Institute of Technology, Arba Minch University, Ethiopia*

Correspondence should be addressed to Milad Mohseni; stu.m.mohseni@iaut.ac.ir
and Bhupesh Kumar Singh; dr.bhupeshkumarsingh@amu.edu.et

Received 11 June 2022; Revised 30 June 2022; Accepted 2 July 2022; Published 9 September 2022

Academic Editor: Samson Jerold Samuel Chelladurai

PCM (phase-change memory) is a memory innovation that has gained prominence as a capacity-class memory for computer systems. It is made up of a tiny functional amount of phase-change material that is located in the middle of two electrodes. In PCM, data is kept by utilizing the difference in electrical resistance between a crystalline phase, which has a high resistance, and its amorphous phase, which has a low resistance. Using electrical pulses, the phase-change material would be shifted from a high to the low conductive region and conversely. However, the device's material science concerned with PCM has been generally studied, and questions remain regarding their electrical, warm, and fundamental aspects since its publication in the 1960s. One major downside of PCM is its low heat conductivity, which causes delays in the energy charging/discharging procedure and hardware efficiency. As a result of this, one of the primary focuses of PCM studies has been the improvement of PCM's heat conductivity through the utilization of nanotechnology and nanomaterials. Nanotechnology has been developing ultrasmall nanoparticles to improve traditional PCMs' thermophysical characteristics. These nanomaterials, such as metal, metal oxide, and carbon, will significantly boost PCM's thermal properties, including supercooling, viscosity, and heat capacity. An overview of PCM devices is presented in this article, which underlies perusing and composition activities. Consequently, we offered novel PCM devices and materials. Therefore, the total study is qualitative, and no machine learning approach is used. Because of this, we cannot say that the data is quantitative. Our work includes both test representations of the specific features observed in nanoscale PCM devices and material science demonstrations. In the end, we provide a point of view on some remaining open inquiries and possible future exploration directions.

1. Introduction

The PCM is a revolutionary technological advancement in the field of nanoelectronics. A PCM contains of lesser capacity of floor switching hardware crammed among two terminals. When the resistance between a glass-like stage and an indistinct low conductivity stage differs, the material changes. Electric flow beats can change the material from a low to a high state of conductivity. The PCM device has electrical interlocks that can be used to retrieve shutdown data [1]. PCM contains PCM lance cells, mainly phase-change materials, metal electrodes, resistive plugs, and transistors. As manufactured, the material is in a high conductance state. It is because the action temperature of the metal-linked layers is abundant to crystallize. In the beginning, the programming region is melted; then, a large electrical current pulse is applied for a short duration to quench it into the amorphous state. Following this, an area of amorphous stain substance will begin to develop inside the PCM cell. For PCM, this amorphous area is in order with low resistance and effectively manages the resistance of the memory unit between electrodes' top and bottom. When the crystallization temperature and heating value are kept at the same degree for a lengthy period of time, the crystallization process can be restarted, and the crystalline condition can be restored [2]. Germanium Antimony Tellurium (GST) alloys are utilized in phase-change memory because they have unique features that allow for nonvolatile storage [3, 4]. Heat can cause the alloy's state to transition into two distinct "phases" (crystalline and amorphous), which is how data is stored. PCM memory has the ability to enable significantly faster write cycles than NAND memory. NAND Flash involves the deletion of data before writing new data, whereas PCM does not, making it faster [5, 6]. Phase-change memory (PCM) can save more data than CDs, DVDs, Blu-ray, etc., in the same space. PCM is a hybrid of flash memory and dynamic random-access memory (DRAM). It has joined the progressively developing nonvolatile industry. It is evolving as storage-class memory (SCM) because of its excellent reliability, density, extended durability, low energy consumption, and faster-operating speed. If the electricity goes off, data can still be accessed and written to this storage. Information is stored in phase transitions [7].

However, one of the key characteristics of PCM is that the set-aside data is kept (generally for ten years at room temperature) and is written in an original format that can be analyzed to inform conclusions [8]. In other words, in order to recover previously saved data, the PCM measures its electrical resistance. With PCM, data is held for a prolonged time (at room temperature, it lasts for up to 10 years) yet can be written into just a very few nanoseconds. Such characteristics potentially allow PCM for NVM like USB (Universal Serial Bus) and hard discs to operate as rapidly as DRAM [2].

One of the most significant considerations about a storage device is that it can store and retrieve data. Data can be stored in phase-change memory by switching crystalline (regulated) to amorphous (irregular) phases of a phase-change material within the memory. Optical and electrical characteristics undergo a major shift due to this process. Amorphous phases have high optical reflectivities and low resistivities, while crystallites have low resistivities and high optical reflectivities. The optical characteristics of PCMs make them ideal for optical disc storage like Blu-ray discs, CDs, and DVDs. Additionally, PCM keeps data using the difference in resistance between the two phases. When writing in PCM, an electrical current is used to change the state of the amorphous material to the crystalline one. Reading the electrical resistance of a PCM gadget is often part of the READ procedure, enabling us to determine whether the gadget is amorphous ("0") or crystallized ("1") [2]. Ever more demanding applications are pushing the limits of MCU designs due to their requirement for more processing power, lower power consumption, and larger memory capacity. One of the most onerous requests is for greater embedded memory, which can hold larger and more intricate firmware [9, 10]. ePCM addresses these chip- and system-level challenges while meeting AEC-Q100 Grade 0 vehicle norms and operating at temperatures up to +165°C. Furthermore, ST's technology protects data with radiation and assures firmware/data retention via high-temperature soldering reflow processes [11, 12]. As a consequence, PCM may be utilized for atypical applications like flash and hard drives, while operating at nearly the same speed as unstable memory including DRAM (Dynamic Random Access Memory). Non-von Neumann recording is an exciting and innovative application for the PCM that is worth exploring further. In this context, memory devices are devices that store data as well as perform specific computations. A standard PC (Personal Computer) is unable to eliminate the need to transfer data between CPUs (Central Processing Unit) and DRAMs [13]. In von Neumann's usual advanced PC, separating data and its offsets becomes a critical bottleneck. Costs, creating things, and compromising the critical level in a computer system have all been concerns in the last ten years, with Intel's productive shipping being a prime example [14].

Figure 1 shows the mushroom-shaped PCM system, which incorporates a level alternate cloth sandwiched between a pinnacle cathode. Optane launched a nonfaulty PCM-inclined memory in 2018 that would be used to replace the current memory storage system. This indicated that PCM could be used as a high-stage memory in staging settings. For this reason, understanding how improvement can happen requires an in-depth knowledge of the actual mystery cadres and kingdom components of the PCM [15]. Moreover, future PCM residences could also be used for applications other than von Neumann. Within the last 50 years, the PCM has investigated electric devices, crystallization frameworks, and herbal stochasticity, which all of them have played an essential role in the PCM's work [16]. Phase-change memory (PCM) is a critical enabler technology for nonvolatile electrical data storage at the nanoscale scale. A PCM device consists of two electrodes and a small active volume of phase-change material [17, 18]. One enticing feature of PCM would be that the recorded data may be kept for a prolonged period while being transcribed in a matter of nanoseconds [19, 20]. A version of the contemporary fabric technology appreciation is

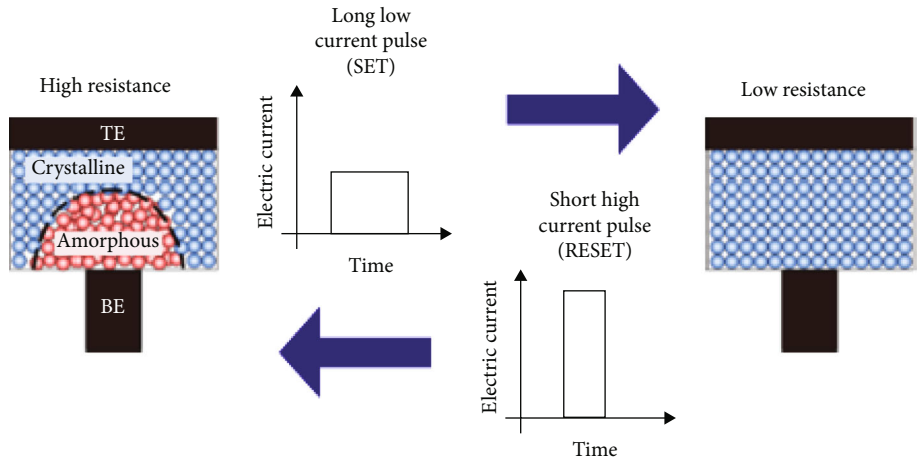

Figure 1: Activity tenet of PCM.

presented in this paper, which supports the WRITE and READ commissions. PCMs have established genuinely novel physics and advanced modeling issues for the industry and new opportunities in nonvolatile memory. A proper explanation of how PCM gadgets work should consider how heat and carriers move in solid crystalline and molten phases that are both present simultaneously, as well as in the amorphous phase where threshold switching, functional relaxations, and crystallization happen. The crystalline phase would be shifted into the amorphous phase by heat-induced melting and rapid cooling, which causes the loss of slow regularity and the formation of a tightly linked material. The transition from an amorphous phase to a crystalline, conductive material state occurs at the threshold voltage (VT), which is 0.6 V. Because of the effect, the amorphous phase can be warmed considerably at a low practical bias, enabling spontaneous crystallization to happen on the millisecond time scale [2].

Crystallization demands a very significant period of time for amorphous glass at ambient temperature. The amorphous substance will quickly crystallize when heated to a sufficient but not melting degree. In order to regain the substance to its amorphous state, it must first be warmed higher than its melting point, and next, it must cool off very quickly. Due to this fast cooling down, the crystalline structure will be "frozen" in an irregular state. When an electric charge is sent through a phase-change material, the heat generated could also be controlled. It is called a RESET or SET operation when an electrical pulse is applied to transition the device from its crystallized state to its amorphous state [2]. In this paper, a two-step SET operation scheme is presented for improving write time in phase-change memory (PCM) systems. In the two-step process, firstly, nanoparticles are initially produced in the form of a dry powder by employing chemical and mechanical processes such as sol-gel, ball milling, and chemical reduction. After this step, the nanoparticle powder formed is combined with the base PCM. The particles are dispersed uniformly by the utilization of a variety of processes, including high shear mixing, ultrasonic bath, and electromagnetic stirring. Figure 2 depicts a schematic illustration of the two-step process. One of the most notable advantages of this technology is the capacity to generate nanostructures for mass production. Nevertheless, this technique suffers from particle agglomeration, which supports the adoption of a single-step preparation procedure [21]. Surfactants have been used to keep particles from sticking together. They do this by making a wall and lowering the surface tension between the base fluid and the particles. They contribute to the design's stability by producing electrostatic repulsion and zeta potential [22]. During the process of creating NePCMs, several studies have made use of a variety of different surfactants. Some of them are Sodium Dodecyl Sulfate (SDS), Sodium Dodecyl Benzene Sulfonate (SDBS), Poly Vinyl Pyrrolidine-40 (PVP), and Ethanol [23–26], respectively. PCM may be used for unusual applications such as flash and hard drives while running at approximately the same speed as unstable memory. A pinnacle cathode is sandwiched between a level alternative cloth in a PCM system. PCM homes might be used for purposes other than von Neumann. PCM is a fundamental enabling technology for nanoscale nonvolatile electrical data storage. A PCM device is made up of two electrodes and a small amount of phase-change material.

During phase 2, we will introduce a PCM framework close to its simple motion guidelines and applications. Section 3 shows an example of a writing process along with warm residences, crystallization, and innate stochasticity. A phase of the READ motion is illustrated by Section 4, as well as the temperature and voltage dependency of electric vehicles, deterrent buoys, and disturbances [27]. The remainder of the paper is arranged as follows: Section 2 offers a summary of previous research on this topic. Section 3 describes the suggested architecture and approach. Chapter 4 consists of experimental data and a comparison of classification methods. Finally, Section 5 discusses the paper's conclusion.

2. Literature Review

2.1. Fundamentals of Phase-Change Recollection. As PCM uses presumed step-by-step mathematical situations, we can switch back and forth between indistinct and glassy instances

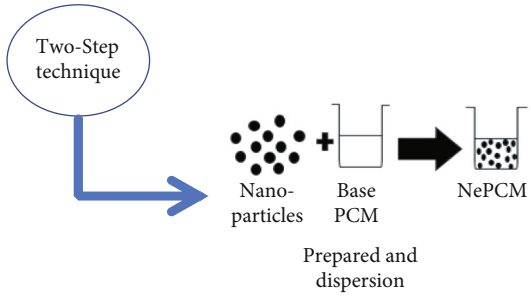

Figure 2: Two-step method diagram.

of electrical resistance, which decrease critical grades [28]. A PCM tool contains a layer of step-converting fabric sandwiched between steel leads (Figure 3). The memory fluctuated when converting STAG fabric, so the low block state's aid was retained without tension. According to Hunt et al., such materials could have been used to create high-performance digital storage cells and transfer rooms in Apple sporting events [28]. In the late 1970s and early 2000s, other attempts to make dependable PCM cells encountered problems due to device decay and instability [29]. Consequently, interest in producing electric storage cells with degree-alternative substances declined. In the 1990s, degree-alternative materials were widely used in optical storage devices, CDs, DVDs, and Blu-ray players. Data is stored in the optical storage by heating the alternate fabric with a laser source to separate the indistinguishable and clear steps [28]. In light of the results of optical accumulation with other surrounding substances, there has been a renewed interest in PCM advancement. A researcher with the name Olshansky in the 2000s and Micron in 2012 began producing PCM chips with different sizes up to 8 GB. Because the boundary is considered a part of the memory, segment shift blending is usually used [30]. It was the first improvement under the Intel Optane brand name broadcast in 2018 and opened steadily as low-capacity, low-clunky volatile memory (16-64 GB).

2.2. Main Control Principles. A storage tool permits the storing and recovery of records. As PCM data is recorded, the expanded material within the storage tool must convert from a glassy status (described above) to an undetectable status (dissolved) in an identical manner.

This variation is a result of the vast difference between electric devices and optics. The indistinguishable desk exhibits excessive resistivity and coffee-like optical reflectivity [28]. The RESET function was used to return the device to the resistance glass state (Figure 3), which is usually recommended due to the SET.

In Figure 3, instead of the strongly glass-forming combinations based entirely on chalcogenides that were used as STAG in the 1970s, today's compounds follow the Get-Sb2Te3 line, which indicates significantly faster recrystallization. Each optical storage device uses a section of alternate material from its own circle of relatives [31]. A common PCM molecular is supplied in sufficient quantity to limit the amount of level alternate material required to obstruct the modern direction through the tool. The device is limited, which makes the memory molecular more incredibly powerful. The component ratio is determined by the cathode length and the number of trapped or restricted cells within the molecular. The bottom anode contact (usually the hottest part) is the fundamental part of the molecule. Generally, all in all, connected cells achieve decreased WRITE flows when compared with dedicated cells for a given interdisciplinary area. As a result, experiments in fundamental studies have investigated the association of such molecules [28]. This molecular association is unusual in terms of place association. Alternating materials, such as surrounding material and higher cathode cloth, are deliberately used to form sublithographic islands in a massive base anode. As a similar notion, the "pore" molecular combines the μ-channel molecular with the linked molecular [32]. There is also a balanced type of memory molecule array called interfacial (ice) PCM, which uses a stack of molded alternate super guide materials connected by interchanging layers of vitreous liquid [33].

The most important requirement for a PCM machine to build up electrical records is high persistence (usually > 108 SET/RESET cycles before it malfunctions). Moreover, the embedded memories are expected to have remarkable flexibility (cycles of perseverance), a RESET of 10 nanoseconds, a SET of 25 nanoseconds, scheduled preservation of ten years at 210 degrees Celsius, and 20-nanometer connectivity. There are many factors involved in PCM machines as a result of their interconnection, such as a breath-taking overview of electrical, warm, and underlying factors [34]. The rectangular form defined in Figure 3 represents the new bodily technological capabilities included with a PCM machine. Electric-powered materials exhibit a strong dependence on voltage and voltage temperature. Figure 4 demonstrates that I is adjusted to a low value with the carried-out voltage (V) and amorphous thickness (U_a) as a percentage of undefined area dimensions. T is the temperature dispersion within the machine, which is part of the third-dimensional directions and also the circumstance of execution of the knowledgeable level indicated in Figure 3 [35]. In addition to the critical thermoelectric effects, the warm shape also possesses the PCM's warm conductive properties on a nanoscale. It suggests a glass, which may require special unwinding residences as well [36]. According to Figure 5, only limited portions of high-priced advanced volatile memory are situated near the CPU using vast minimum expense measures. This gradual capability applies to inventory data, however. A large gap exists between memory and capability in getting access to the season of round 3. It is probably filled with alleged "stockpiles of elegance memories."

2.3. Functions of Phase-Change Recollection

2.3.1. Memory Machinery. In most cases, memory motion methods should match the CPUs' runtime openness with slower memory, increasing the limit. For developing purposes, the configuration must be stable [36]. As illustrated in Figure 5, because there is less power and a negligible cost at this stage, the access times are significantly slower than during CPU exercises. Tape drives and Hard Disk Drives (HDDs) benefit from NAND (Not AND) gate flash memory

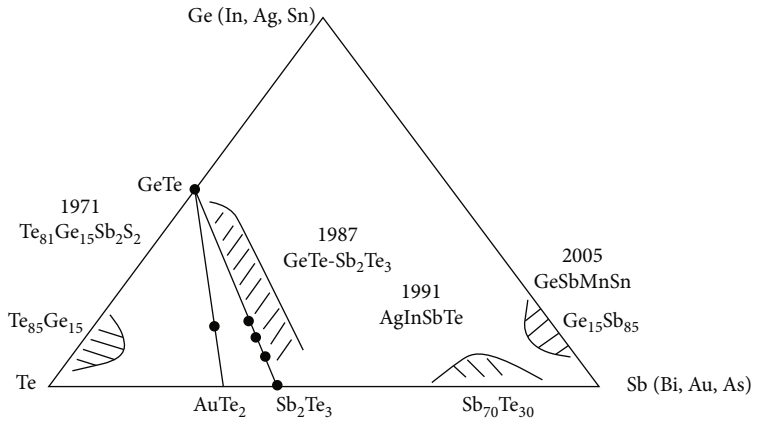

Figure 3: Most utilized stage change raw material for PCM and optical stockpiling. Republished with consent from Springer Nature: Nature Materials Copyright (2007) [14].

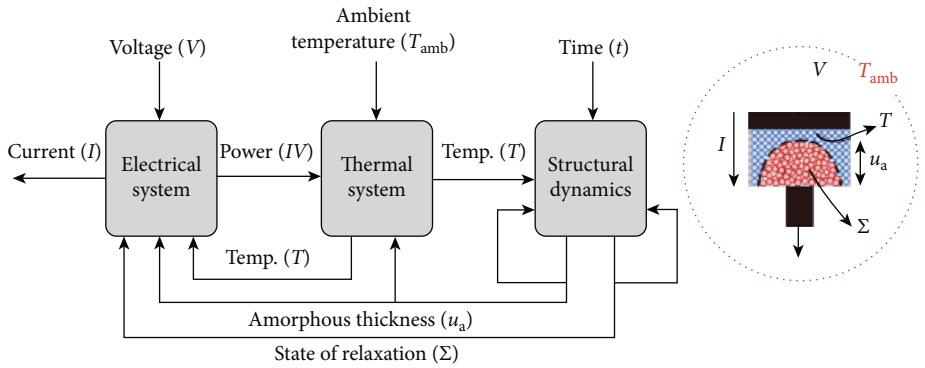

Figure 4: Block diagram of interconnections between electrical, thermal, and structural dynamics in a PCM device.

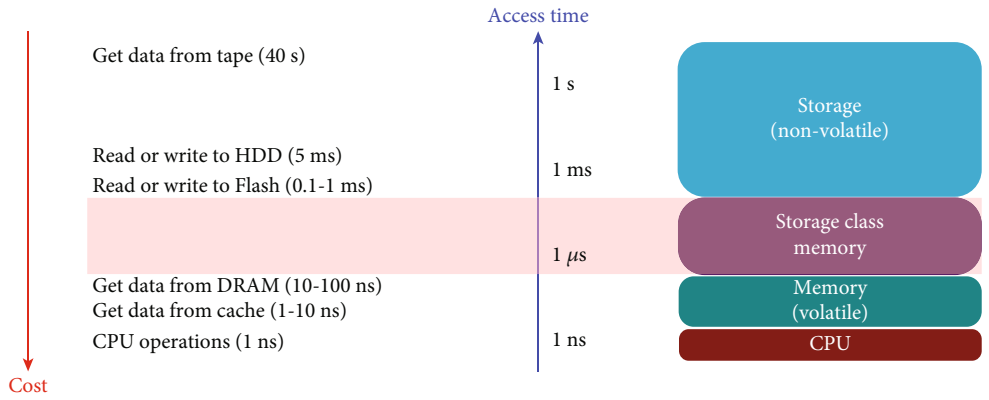

Figure 5: Access instances for unique reminiscence and capability innovations.

and NOR (Not OR) fuses. Additionally, memory improvements can be costly (information is misplaced when strength is slowed), but they have greatly reduced access times. SRAM (Static Random Access Memory) used for processor backups is combined with DRAM (Dynamic Random Access Memory) to form an off-chip memory [37]. PCM has been studied in a large number of papers for over 10 years as a capability alternative to DRAM. As per the number one opinion, DRAM lags behind NAND Flash and CMOS (complementary metal-oxide-semiconductor) because of the downsizing on the 45 nm improvement middle and incompatibility [38]. There is evidence that PCM reduces in the 20 nm middle, at least from the 32 nm middle. In order to prevent problems with DRAM capacitors from being reduced, the PCM also increased boom head thickness while constantly retaining the charge. Despite the reduced downtime, if PCM can

be thicker than DRAM, numerous improvements to the memory machine's fundamental shape should create PCM a sustainable substitute to DRAM, particularly in terms of preventing and irritating the skin's lifespan. The noninstability of PCM can be exploited in crucial memory to minimize alterations after every authorization, which are inevitable with DRAM. However, at the time of creation, in DDR DRAM, the crucial factors dropped to near 10 nm, indicating a significant improvement in both the 10 nm and 19 nm classes. Because of these new advances in DRAM organization, it is currently unknown whether or not the PCM will require unplugging, especially in terms of stability and reliability. A Storage Class Memory (SCM) is also common for PCM as a superior popular memory. Figure 5 shows a three-degree gap between the transition times of DRAM and flash memory [39]. With respect to these irritations and open costs, SCM with PCM is probably practical. SCM combines the advantages of solid-nation memory, which includes occurrences and strength, with the recorded abilities and low cost of an inflexible circle. SCMs should have a quick SSD (Solid-State Drive) with higher community consistency, as well as faster access times than flash-based SSDs. There can be constraints to entering instances for 1 s competently, but a thick layer will be most significant at a low price. There should be another range that evolves into the age of 100 ns with low strength and price requirements [39].

2.3.2. Non-von Neumann Computing. The Nonong-Neumann element is important for resistive storage devices, as well as PCM. Smooth calculation angles store data and perform switching obligations by using controlled memory and recording. It should be energy-saving and suitable for stable storage devices and can be processed at the nanoscale. There could be a blurring of the distinction between memory and registry, which could result in new computing processes. Estimates and models could benefit from non-Neumann plans because non-Neumann computation fashions use more tolerant devices.

Moreover, innovative devices are used to implement neuromorphic systems for involvement. A remarkable memory management feature is using tolerant devices' actual properties and region attributes for direct device registration. In programs that are no longer Neumann-defined, database PCM devices can exist in a large type of state (within the PCM running standard). A second vital feature of the PCM is that its location can be legitimately determined using electric impulses. Besides reflecting synaptic activity, the PCM (which attaches itself to the current flowing through it) can also perform some computations. It is noted that those chips are used to study scaling data. The storage tool code encoded a scalar value into the optical individual's path as a fundamental step length. Studies have shown that PCM is capable of playing a pivotal role in a John von Neumann practice machine [39].

Figure 5 shows a limited factor model that shows the optimal temperature in a mushroom-type PCM for delivering a high voltage. Near the bottom cathode, the temperatures are high because of the high temperatures in the region. A green heat opposition can depict the negative effects of hot weather. It captures any obstructions to warm temperature pathways in this manner.

2.4. Nanoparticle Improvement on PCM. The poor heating rate of pure PCMs, which reduces the energy capacity, is a significant threat to the broad deployment of PCM energy. Nanoparticles have lately gained interest in improving PCM heat conductivity while retaining higher storage capacity or charging/discharging cycles. Nanoparticles increase PCM thermal performance by distributing particles, enabling a greater charging rate. Consequently, nanomaterials accelerate the phase transition procedure [40].

According to Lan et al., PCM thermal conductivity was increased by 46% with the addition of multiwalled carbon nanotubes (MWCNTs) [30]. MWCNT-PCM nanocomposites were combined with potassium hydroxide (KOH) to improve their distribution in palmitic acid. The modification of MWCNT substrates with grafted –OH groups increases the stability and consistency of PCM nanocomposites. For MWCNT-palmitic acid nanocomposite with 1 wt% MWCNT loadings, the k values rose up by 46% (in a solid form at 25°C) and 38% (in a liquid state at 65°C) [41].

The heat capacity of PCM was improved by graphene to 140% [42]. Doping graphene into a PCM device (1-octadecanoic) improves its temperature (K). The thermal characteristics of PCM materials comprised of Ag nanowires and MWCNTs are compared to those of graphene PCM. With 4 wt% nanofiller loadings, the k value of the PCM material goes up by 2.5 times, or 140%, to 0.91 W/mK. However, the underlying heating value drops down by 15.4%, from 0.38 W/mK for pure PCM.

Tong et al. employed SiO_2 to improve PCM thermal conductivity [43]. Tong used polymeric melamine-urea-formaldehyde to make microparticles of PCM paraffin in place. In order to change the PCM microparticles, graphite and nano-SiO_2 were both included. It became observed that 80% of the paraffin could be put into microparticles without changing its thermal properties. Tong et al. strengthened the architectural bonding strength by adding nano-SiO_2. This made the microparticles robust to high temperatures and had a strong ability to dissolve. The incorporation of nanoparticles had a direct influence on the k value, as evidenced by the considerable increase in melting time.

AgNPs reinforced the walls of microparticles, according to Song et al. [44]. Bromohexadecane PCM's polymer walls were improved by doping silver Ag nanoparticles, which created a robust shape that was more resistant to heat. When combined with polymeric microcapsules with a high surface-to-area ratio, Ag nanoparticles produce a composite material layer with high resilience to polymer degradation during the rigorous production process [44].

3. Methodology

3.1. Thermal Characteristics. If an electrical pulse is applied to a PCM device during a maternal stage cycle, the effects of the device are rarely influenced by the temperature spread. Temperatures close to the base station are abnormally high during

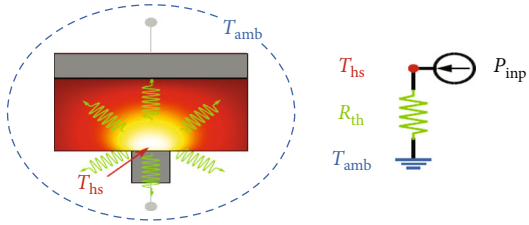

Figure 6: The PCM is a device that operates internally and encompasses temperature, T_{amb}.

the maternal stage cycle. Indirectly, this is due to the fundamental inequality between the upper and lower cathodes. Electricity dissipates, causing urea to be modified by glow transport away from the device [45]. According to its geometric conductivity and properties, ordinary thermal resistance (T_{hs}) corresponds to remote glare (Figure 6).

$$T_{hs} = R_{th}P_{inp} + T_{amb}, \tag{1}$$

where R is the resource, T is time, P_{inp} is the interval, and T_{amb} is the time duration. Thomson's thermoelectric oscillation at the impact of a PCM device causes the impurity area to move along its course.

In maximum step alternate materials, such as $Ge_2Sb_2Te_5$, the Seebeck coefficient is p-type, and the temperature dependence is poor, which results in a low Thomson coefficient. The Thomson impact will create more brightness if j is within the temperature factor from the top anode to the gap of an activity. It widens the hole and expands the undefined area. As a result, much less energy is predicted to reach the start of the first peak, whereas the voltage drop restriction on the pinnacle anode is high compared to the bottom terminal [46, 47].

3.2. SET/RESET Operation. According to Figure 6, the WRITE action of the PCM hides the values of summation and amorphization. It is noted that Joule heating up indicates the state of the PCM device in terms of values above the heating warmth, melting, and state change material [48]. It eliminates all of the previously created discontinuous atomic designs. If the extruded material is fluid, it needs to be cooled to "freeze" atomic modification in a dense region. Consider that the association of fast crystallization (Figure 7) is immediately blocked by rapid reduction. In this case, atomic transportability at temperatures below this shape is low because the debris is unable to improve and discover its most remarkable security [49]. The material is then cooled and frozen in a solid state [50].

3.2.1. Crystallization Kinetics. Development can pressure crystallization if the charge is high enough to allow primary development to the vague clean interface (as shown in Figure 7. In the second argument for the significance of nucleation in PCM devices, if fresh devices can work through the crystallization collaboration and if they can be added to the large, hardened facilities already in place, the entire process can be sped up [51, 52]. For the maximum part, the generic version represents the temperature dependence of the development of the gemstone, in equation (2) [53], where $4r_{atom}$ is atomic compass, λ diffusion rebound distance, R_{hyd} hydrodynamic range, K_B Boltzmann consistent, and T temperature.

$$V_g(T) = \frac{4r_{atom} \times K_B T}{3\pi\lambda^2 R_{hyd}} \times \frac{1}{\eta(T)} \times \left[1 - \exp\left(\frac{\Delta G(T)}{K_B T}\right)\right]. \tag{2}$$

Also, thickness is $\eta(T)$. It is the value that controls crystallization interaction, adapts the necessary stimulus, and couples the Stokes-Einstein condition to the atomic diffusivity. Cooling below the dissolution temperature will reliably raise the consistency as it cools, and it becomes harder to check all feasible plans for a positive temperature.

For equation (3), $\Delta G(T)$ can be more than zero for T condense, meaning the liquid degree is more secure than a glassy degree [54]. Thompson Spacemen Gauge is the verbalization of ΔG, which is often used for degree alternate substances.

$$\Delta G(T) = \Delta H_m \times \frac{T_{melt} - T}{T_{melt}} \times \frac{2T}{T_{melt} + T}. \tag{3}$$

In equation (4), m means fineness [55]. T stands for the time interval, and T_ϑ stands for duration capacity. For example, two papers describe embrittlement recorded as hard copies ranging from 20 for solid drinks containing SiO_2 to over 154, often regular polymers [55].

$$m = \frac{\theta \log_{10}\eta(T)}{\theta(T_\vartheta/T)} \lceil T - T_\vartheta. \tag{4}$$

3.3. Threshold Switching Process. Figure 8 depicts low-discipline competition as part of a PCM device's implemented programming ability at the start of the RESET procedure. Using PCM for electrical data storage requires the crystallization/amorphization scheme below. On the left, the undefined primary quarter is constantly created to take shape until the low-discipline competition is predicted to grow programming energy [56]. It is essential to be able to quickly increase the temperature inside the device without a reservation by the limiting region. A high-quality energy laser source is used to efficiently heat the stage-converting material within the optical restriction, irrespective of the material's area [57]. One of the primary characteristics of PCM that provides a fast and spectacular shift of energy is its use of a comparatively low-voltage pulse generated by a nonlinear multiplicative voltage.

Figure 8 shows a nonlinear voltage shape in the presumed OFF region (or subthreshold shape), which indicates that super momentum is ohmic as the implemented voltage increases [58]. As the selected voltage Vth increases, the on-the-spot invitation of the doubtful area will increase rapidly, resulting in a poor differential in opposition to skin breakdown. The PCM works in a group, and the horrible

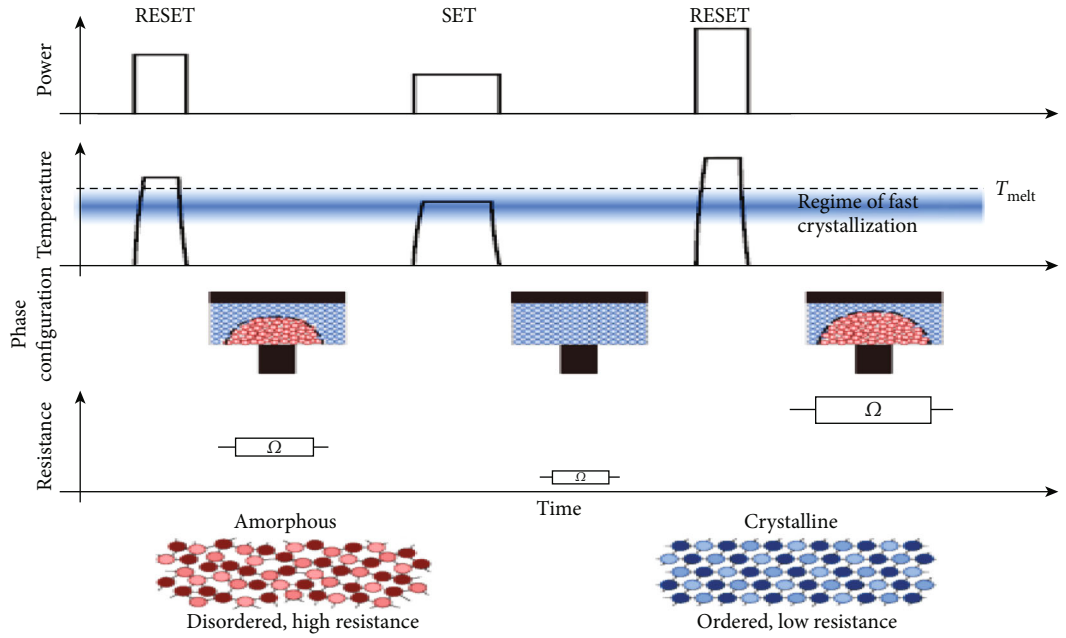

Figure 7: The standards of a WRITE activity in PCM. A RESET in PCM device reaches the highest obstruction area by heating the extruded material over the melting.

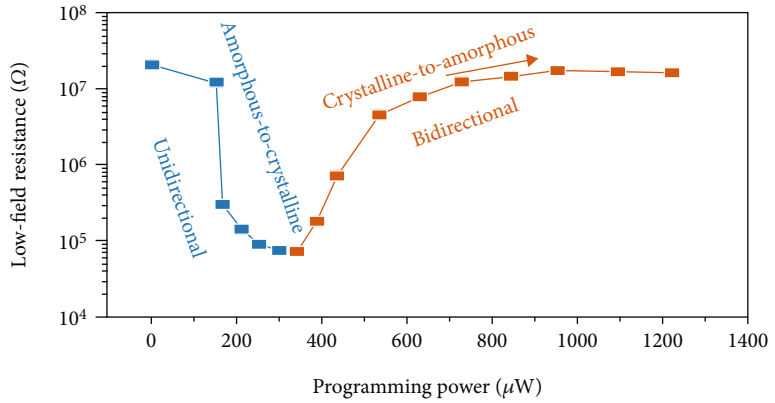

Figure 8: Low-discipline competition as part of the implemented programming power for a PCM device at the beginning of the RESET process.

differential resistance may be pushed by employing nonlinear selection equipment or the semiconductor in collection with the PCM [59]. The current voltage will increase rapidly when connected to V_{th}, causing the voltage to reverse. The device's resistance collapses below zero on the change restrict, resulting in poor differential prevention in the area. The I-V mark is developed from the glassy state using improved voltages in the simple line. High temperatures cause the degree of fabric to melt and eventually break [60].

3.3.1. Thermal Models. Due to the recent launch of the devices, significant conductivity will grow as the temperature rises within the device. By increasing the conductivity, the device will achieve an extended electricity dispersion, resulting in additional growth in the conductivity [61]. Consequently, this may result in a weak spot in this notably nonlinear statistical structure, resulting in a low differential I-V rating. Electric oscillations were proposed as the primary device to explain facet-to-face alternate materials. In 1922, Wagner proposed the warm failure circumstance. In his study, he used a temperature-dependent dielectric layer of thickness L. When the layer broke, it had to be like a thin fiber with a transverse region, which allowed the glow to pass through.

$$\sigma(T) = \sigma_0 \exp\left(\frac{-E_\alpha}{K_B T}\right), \tag{5}$$

$$SL\sigma(T)F^2 = \lambda(T - T_{amb}). \tag{6}$$

According to equation (6), L denotes the thickness of the layer, F the electric field, λ the warmth exchange coefficient, T the fibre temperature, and T_{amb} the ambient temperature. In the preceding scenario, solving for $\partial F/\partial T = 0$ yields the edge temperature at T_{th} in which I–V becomes a negative differential.

In equation (7), $E_\alpha \gg 4K_B T_{\text{amb}}$ is assumed to hold true. A differential conductivity of $E_\alpha < 4K_B T_{\text{amb}}$ cannot be negative. Electric field F_{th} relating to this state is agreed by equation (8).

$$T_{\text{th}} = \frac{E_\alpha}{2K_B}\left(1 - \sqrt{1 - \frac{4K_B T_{\text{amb}}}{E_\alpha}} \approx T_{\text{amb}} + \frac{K_B T_{\text{amb}}^2}{E_\alpha}, \quad (7)\right.$$

$$F_{\text{th}} \approx \sqrt{\frac{\lambda K_B T_{\text{amb}}^2}{SL\sigma 0 E_a}} \exp\left(\frac{E_\alpha}{2K_B T_{\text{amb}}} - \frac{1}{2}\right). \quad (8)$$

For unpredictable state failure, the luminescent equilibrium condition assumes the project where C is the thickness. When the state failure is unpredictable, thermal equilibrium assumes the thickness (L), and C is the specific heat. According to equation (9), when conductivity has a field dependency $I(F, T)$, the model is classically interpreted as electrothermal due to how they approach hot effects. Field-dependent conductivity is caused by these electronic cycles. Various authors [62] proposed electroweld models to explain edge trade-in in chalcogenide glasses. As a result, they were largely abandoned during the 1980s for some electronic excitement. However, thermally initiated trading has been reevaluated when supervising nanoscale PCM gear, in which the effects of self-heating are expected to be significant.

$$\rho C \frac{dT}{dt} = \alpha(T)F^2 - \frac{\lambda(T - T_{\text{amb}})}{SL}. \quad (9)$$

3.3.2. Electronic Models. An essential technique for enhancing the effect of exchanges in electronic is the double implantation version that is implemented in an obvious way using Mott and Heinisch [63]. After a voltage is applied throughout the device's terminals, electrons and currents can only pass via the cathode and anode. After that, the blended transporters reunite with the mass [64].

3.3.3. Invention-Recombination Model. In the first step, the valence variation pair (VAP) imperfection model, first developed for accidental chalcogenides, underpins Adler age recombination. Under isothermal circumstances, for example, a boundary change can occur at some point of vibration ionization. Numerous conductivity, openings, and imperfections must be considered to achieve conductivity in an electric area. In the second step and according to equations (10) and (11), G is believed to be the fixation of the transporter and $g(F)$ is the humdrum growth ability of the electrical area [65]. The solution for this version can be derived inside the deactivated state, where the loose transporter technique is significantly more modest than clustering seizing processes and considering a single transporter model (P).

$$G = \frac{P - P_0}{\tau_p}. \quad (10)$$

The frame may be composed as follows, where τ_p is the characteristic hole capture time and P_0 is Gatherum. Equation (11) solves this equation because $g(F)\tau_p$.

$$p = \frac{P_0}{1 - g(F)\tau_p}. \quad (11)$$

Ft, which satisfies the condition $g(F)\tau_p = 1$, is the field in which the edge exchange occurs. Similarly, free electrons and opening clustering are currently greater than centralized capture foci in the postignition state. Raišienė et al. presented a great arrangement of this model with information about the tests in detail [66]. Nanoscale PCM cells are enhanced by assuming that reconnecting occurs exclusively in focus defects. As a result, it can improve the model's strength beyond VAP speculation by incorporating distortion expressions that serve the same purpose (such as cell traps). There is also discussion about the validity of using an age-type ionization instrument for indefinite semiconductors, where most of the pores are tiny.

3.3.4. Tunneling between Trap States. According to Elmina, the change in Fowler-Northeim Tebow from massive to shallow Tebow causes instability at excessive fields because the tunnel modern will decrease compared to the thermally precipitated current. As a conduction version, the current is symbolized by the Poole-Frenkel oscillation (see Figure 9. a) from different states (superficial and extensive). In common, electrons accumulate in a region extending to this floor; for this reason, the semiarrested stage of electrons moves to the ton band when the relationship with electrons in this region is developed. As the twin blend version, infiltration has been identified via the Fowler-Northeim tunnel [67]. This longer period terminates all the available quantity of section material, although this version would produce an awful IV Chirac to the differential. This is because the current must be greater than thermally precipitated current (piano Librium) in order to communicate instabilities that may lead to exchanges [65].

3.3.5. Hot-Carrier Model. Elmina's second version is used, which was later modified using a hydrodynamic machine. Fermi movement that combines a semiorganization stage and a temperature vector replaces the equilibrium Fermi transport. Strength equilibrium can tolerate coordinate independence and ohmic conduction [68]. One possibility behind this research area is that the longer provided instances are likely to be beaten with parasitic completions to both the tool and the electric-control circuit. Additionally, complete development of the hydrodynamic automobile concept among nebulous silicon professionals is no longer available.

3.3.6. Field-Induced Nucleation. According to the version of noncoactivity elicited by using the Kirov area, there is no limit to delivering an electric-powered area on the strength. Therefore, hole gems are formed rapidly in an excessive electric area. Consequently, an electric-powered area can create a fiber that can move from one anode to another within a predetermined timeframe. A device has switched when its fiber touches each cathode. When the sphere is removed, the fiber will diminish or increase based on whether its amplitude is less than or more than the simple thermodynamically strong range. If the fiber is thermodynamically strong, it avoids the reminiscence trade; it shows the opposite extrude within the blocked state. This version has been visualized to quantitatively depict the exclusive trade time's temperature and voltage dependence. One debate is whether real sensible limits can include mimicking the trade at tentatively anticipated electric-powered fields.

3.3.7. Experimental Characterization. A PCM device's edge switching capabilities depend on a number of parameters. The edge voltage is a basic reliance on the customized obstruction state. Figure 9 illustrates the relationship between edge voltage, current additives, and the altered voltage offered by the PCM device to reset it. As RESET current grows, the initial voltage factor will correspondingly increase with the identical room size extension. With an increasing RESET current, the device begins to switch lower until it reaches a consistent value of about 10 μA.

In most cases, the cutoff voltage does not change much with temperature and can be decreased virtually, while the crop will increase much less than best from room temperature to 123. As time passes, the tension in the area will also rise due to the important launch of the fog segment, which works to catch the glide (Figure 10). As shown along with the look at statistics, the reenactments were completed by simply replacing the thermally assisted restriction. Initially, information was recreated from small collections of information within the RESET region. The composition also proved a long duration of stochastic patterns. In spite of the fact that more than 50 years after the surprise was first embedded within the material, no intelligent shape has yet been proposed to quantify all the alternate cutoff options conventionally visible on fabric and devices in a united manner. Chalcogenide devices (typically small films) have encountered many logical inconsistencies with a single warm industrial part, especially in thin materials; the query of whether the regulations of the alternate mechanism of the recent or digital breaking factor stays open. AIST level fabric showed fast switching instances (sub-nanoseconds), which led one to question whether this device requires a warm alternative material. According to tool structures, beneficial materials, or other conditions, some components may have more significance than others, and determining how they work will yield the most likely arrangement. In addition to giving attention to further decoupling of warm and digital-best outcomes in research, this might be another area where progress is needed. An electric-powered region can generate a fibre that can migrate from one anode to another in a specified amount of time. When a device's fibre reaches each cathode, it has switched. When the sphere is removed, the fiber's amplitude will decrease or rise depending on whether it is less than or more than the simple thermodynamically strong range. The edge switching capabilities of a PCM device are determined by a variety of characteristics. The edge voltage is fundamentally dependent on the tailored obstruction condition. Most of the time, the cutoff voltage does not change much with temperature and may be virtually reduced, although the crop will increase much less than ideal from room temperature.

3.4. Write Stochasticity. In the present study, stochastics used of the PCM change measure, break-factor change, and the set ton measure here. Stochastics of PCM community trading can be exploited specifically by individuals who code in top neural associations or by people of diverse ages for stochastic treatment and cryptography. As a result of the setting up of various PCM devices, we are able to carry out a positive heartbeat p (zero P_1). We can adjust p to the desired value by modifying the sufficient stroke or stroke width (Figure 11).

3.4.1. Threshold Switching Stochasticity. Figure 12(a) presents the delegate opinions of the stochastics of the breakpoint in a PCM device with a unique breakpoint. After a voltage pulse is applied, it takes a certain amount of time for the current to increase at once. The PCM device is easy to peer into and allows every experiment to achieve alternate current monitoring, providing a unique time and a few variables. The consequences are proven in Figure 12(b). In all three of the cases, the discretionary lag time variable aligns with the right log-ton. Widespread use of the version provided could effectively produce the distributions that were likely to be assessed by inserting a small (0.5 percent) anomaly.

The device's formless thickness and enactment energy after RESET. This study shows how varieties can clarify the stochasticity in limit-exchanging cycles in nuclear setups of the undefined stage produced by RESET interactions with positive beat width.

3.4.2. Memory Switching Stochasticity. The 2nd supply of stochastics for PCM comes from the crystallization cycle. As shown in Figure 1, the mushroom-kind nanoscale PCM tool is ruled by the reinforcement of the nanoparticles. Since the transparent vitreous region and, even more, the sufficient pulse amplitudes, the temperature is ruled by a voltage surge significantly similar to the current flowing into the tool's interior. As a result, the material is even more powerful than the glass within the vague interface. As a result, even small variations within the indistinct extent of atomic preparations performed in RESET can cause distributions within the convincing undefined thickness, resulting in a stochastic development of the crystallization duration of a PCM component. Figure 13 shows the overall performance time of the PCM scream. According to experts, a PCM device needs to be rebooted before it can be set up with an appropriate heart rate. Due to this

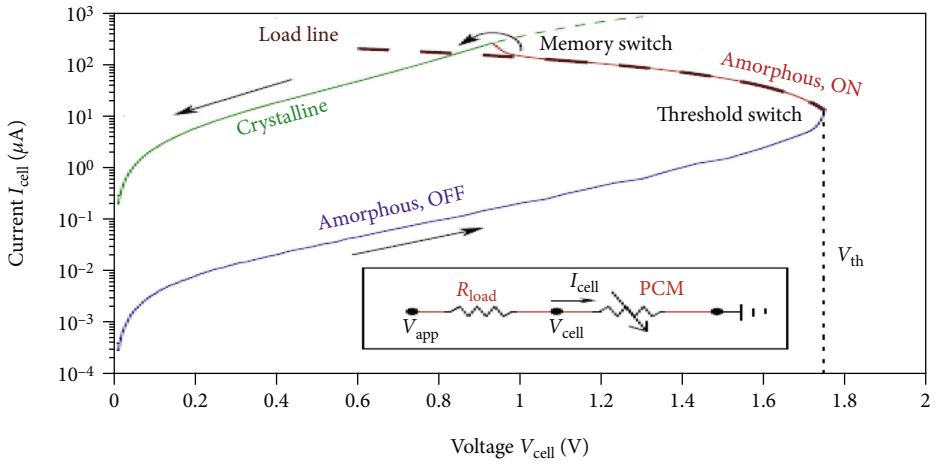

Figure 9: Semistatic trading I–V nature of a PCM contraption at first in the indistinct state assessed in voltage mode.

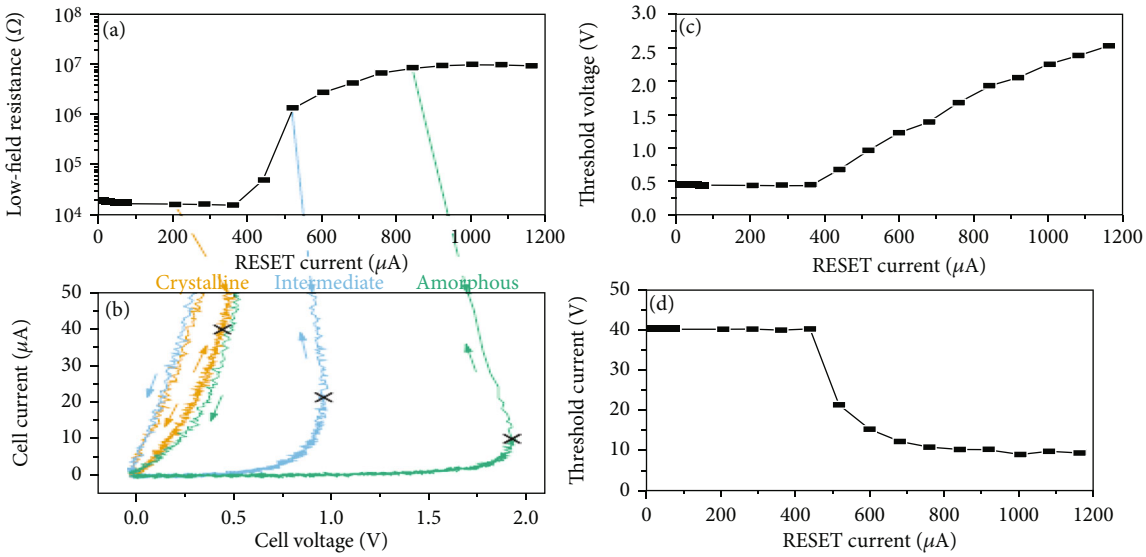

Figure 10: (a) Change in low-area resistance while making use of step by step better RESET currents. (b) Measured I–V traits after RESET for 3 extraordinary resistance states.

scatter, the number of Christ pulses can acclimatize so that the equipment can adjust to a given possibility p for a.

4. Result and Discussion

Generally, the READ operation in PCM involves testing the resistance of the PCM device using a low-voltage shock. Figure 13(a) shows V mappings for the three new reserve states. With time and temperature, the resistors retrieve reserved information, and it causes phase-change material in the mist state to generate these clusters of obstacles. The low-field resistance at room temperature is generally evaluated in Figure 14(b). Generally, the resistance increases over time, which is consistent with block drift.

Consequently, different resistances are difficult to detect. In both cases, there is massive resistance instability after an ideal opportunity for higher deterrence. It is also another critical test for stunning limits, usually attributed to the undefined stage. As subsections proceed, the PCM resistance will be dependent on voltage and temperature, and a deterrent buoy will also be present. Additionally, the disturbance will be attributed to the vague stage, which is another vital test for determining limits [68].

4.1. Subthreshold Electrical Transport

4.1.1. Temperature Dependence. Both constrained and prolonged states can occur in disordered materials. Amplification and transmission events can be used to determine that a mentioned fulfillment can competently determine low-area conductivity opinions at temperatures above 200 K.

Nevertheless, tunneling at lower temperatures has more power than transporting materials; at room temperature or better, the build-up power for conduction is nearly the

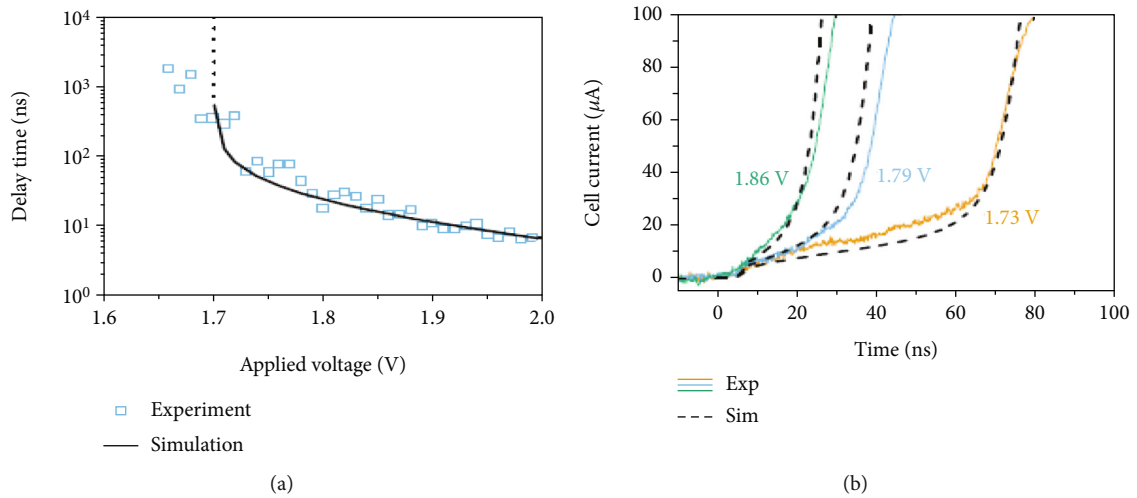

Figure 11: (a) Deferred time as a function of implemented voltage. (b) Current is obtained as a function of time for three different implementation voltages.

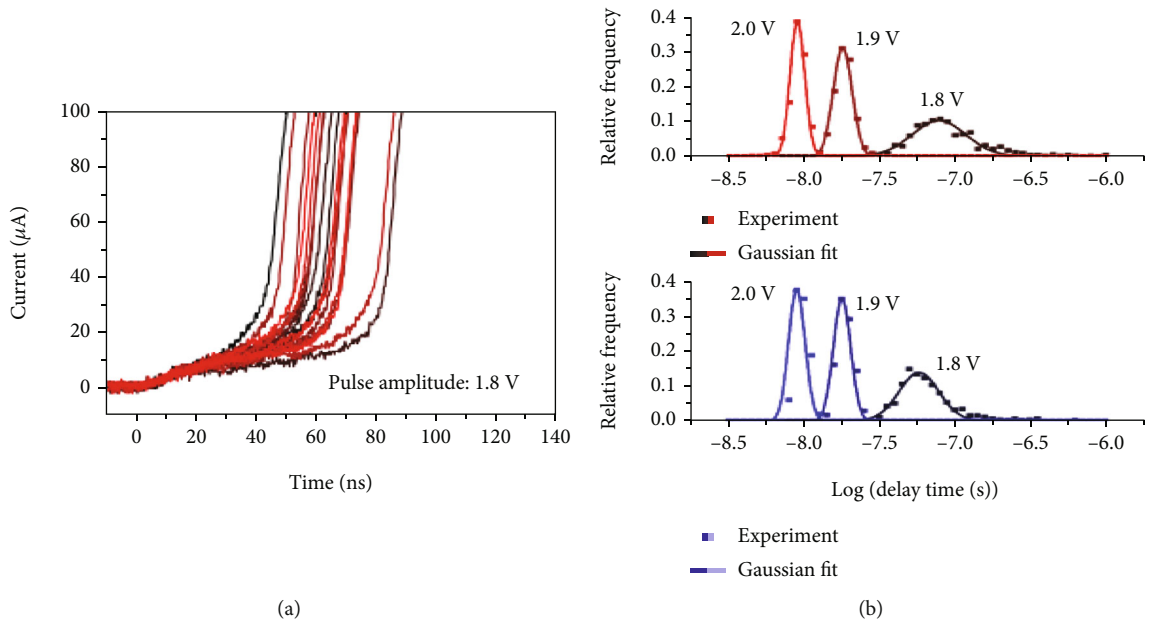

Figure 12: (a) Time vs. current plot. (b) Log vs. relative frequency plot.

optical bandgap. This force power is generally between 0.2 eV and 0.4 eV for undefined PCM. Conductivity arises simplest from unbound electrons and openings that are at or beyond their comfort zone. In the conduction band, electrons are strengthened and expanded by using an electric-powered area with specific compactness. In addition, the openings within the valence band can pass with flexibility. According to Fermi-Dirac measurements, n is the sum of free electrons, and p is the number of open holes within organizations. So, the conductivity relies on the Fermi stage to determine the degree of versatility. A comparison between tape shipping daily and the detection of numerous features shows that in the latter case, the Fermi stage appears low due to constrained states. There is a possibility that nearby debris will discolor the rim of the tape, causing the tape tails to rot severely within the restricted tape. With distance, the features of the wave rot dramatically within these extensions of the band. In general semiconductors, it is possible to get a fringe of the band, semiconductors can create fringes of the band and deep Gaussian states (near the middle of the band-gap). Semiconductors' conductivity grows at certain levels. In contrast, deep traps reduce conductivity by keeping the Fermi stage outside the forbidden band and acting as a site for electron recombination and aperture recombination). Examinations confirmed that each band tail and Gaussian states are available in getting vague [58].

$$\sigma = \sigma o \exp\left(-\frac{E_a}{K_B T}\right). \tag{12}$$

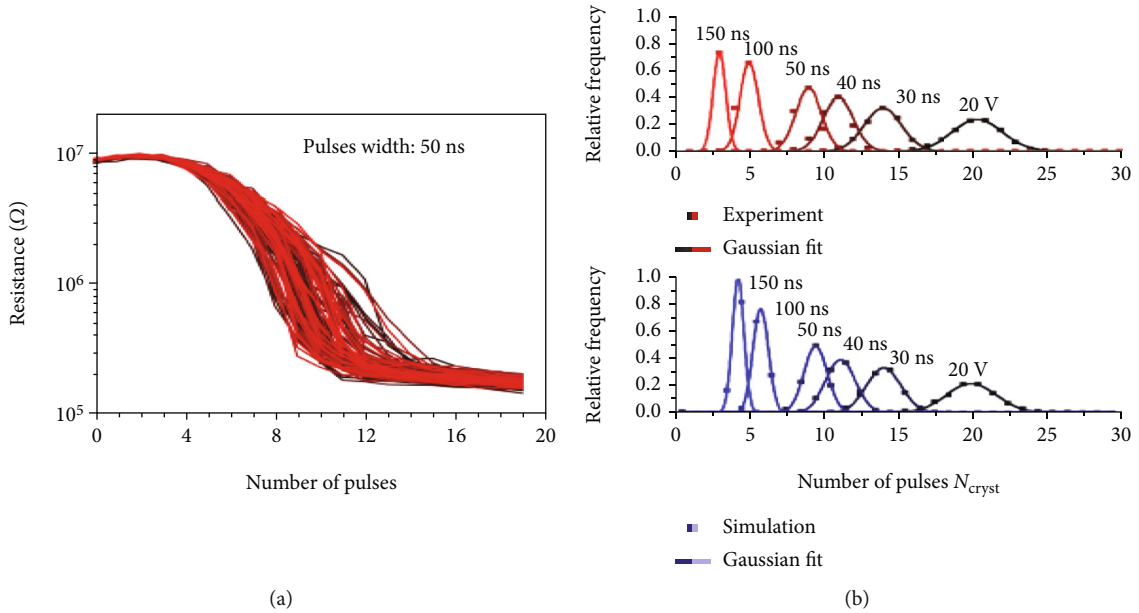

Figure 13: (a) Experimentally measured obstruction as an integral part of crystallization beats for a 50 ns proper heartbeat width. The investigation was carried out multiple times, and the device was reset in the middle of every test. (b) Experimental and mimicked Christ appropriations for six diverse heartbeat widths based on 1000 estimations. Information from [23].

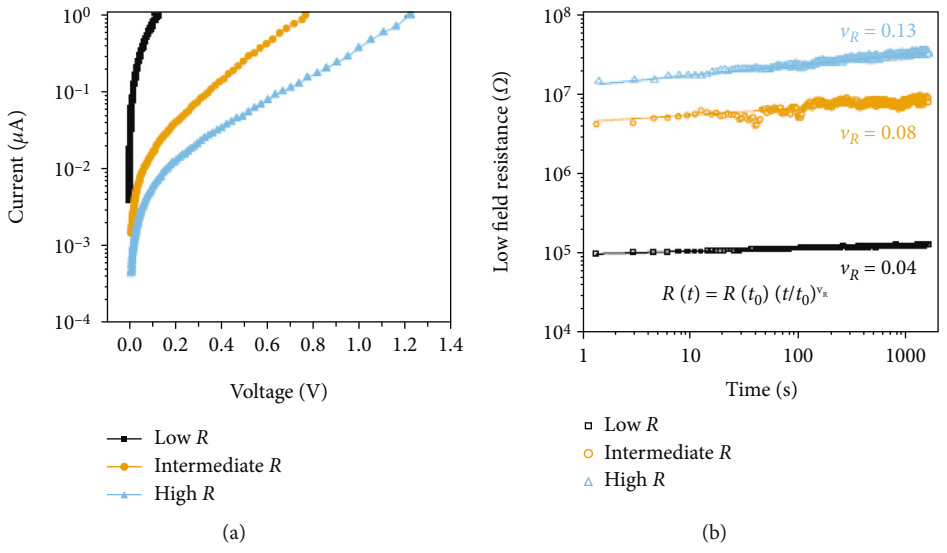

Figure 14: (a) I–V qualities of 3 distinct opposition conditions (low, middle of the road, and high). As the size of the undefined locale grows, low-field obstruction rises, slant of log (I) versus V declines. (b) Resistance depends on time for three diverse obstruction states.

In equation (12), E_a is the stimulation electricity for conduction (the difference between the Fermi degree and the brink of compactness). It may be dependent on the temperature if Fermi degrees change with temperature. Large traps repair the Fermi level in an unpredictably high state of ~0, three eV compared to the edge of the valence band. This distinction is no longer valid for all alternate section materials due to the temperature dependence of the distance E. The Varshney formula is normally used to define this temperature dependence in bulk vitreous semiconductors.

$$E_g = E_0 - \frac{AT^2}{B+T} \approx E_0 - X\,T^2\,(T \ll B). \tag{13}$$

Furthermore, it has been demonstrated that the latter indicator properly indicates the temperature dependency of the optical band hole in step alternative substances. Through Einstein's association, leaping in low subject conditions remains easy in the air (equation (14)).

$$d\sigma h = e\mu h\, N(E_i) f(E_i) dE_i. \tag{14}$$

The chance of a jump is from site i to site j, and the thickness of empty states is j. Therefore, a major challenge is to identify appropriate intersections in r_{ij}.

$$\mu_h = \frac{eD}{K_B T}. \tag{15}$$

Various expressions have been proposed in the literature, which is reviewed below.

$$D = \frac{1}{6}\int V_{ij} r_{ij}^2 N(E_j)\left[1 - f(E_j)\right] dE_j. \tag{16}$$

Additionally, materials that have changed the landscape such as Get and Ge2Sb2Te5, can also be detected as electrically conductive on the conveyor belt. It absorbs temperatures below about 0.200 K, whereby a single authorized direct line is no longer able to represent the low-field conductivity.

4.1.2. Voltage Dependence. A further overview of the data status on subliminal conduction in unclear step-change materials is presented in *i*. A voltage below the commercial limit voltage is designated as *H*. Devices are made in an extended state, relying on tolerance. Around 200 materials royally change the surroundings at higher temperatures. Consequently, it is relevant to technically meaningful applications where an effect occurs at room temperature or higher. Furthermore, we suggest that the examiner composes.

The device consists of the Schottky gearbox or confined spatial extrude regarding experimental results. Poole-Frenkel oscillations are often used in conducting materials with electrical areas within various snapshots. In this version, distortions of extensive molecules provide a Coulomb potential based on the new launch of distortions of large molecules. The ionization power is then reduced within the Electro-deceleration region via the use of $\beta F^{1/2}$ with $\beta = e^2/\sqrt{e\pi\varepsilon\varepsilon 0}$, in which F is applied electric powered region, e is digital charge, and $\varepsilon 0$ is the vacuum that allows a trinity or most likely a dependable repeating dielectric (equation (17)). It must comply with Poole-Frenkel law (conductivity) and depend on conductivity to comply with a design law (Poole-Frenkel).

$$\sigma_{\mathrm{PF}}(F) = \sigma_0^{\mathrm{PF}} \exp\left(\frac{\beta F^{1/2}}{K_B T}\right). \tag{17}$$

One of the Coulomb prospects has a remarkable recovery just where the deformation area is close to one another. Using two middle Coulomb capabilities, it has been shown that the ionization power bringing downward on the area is $(eFs/2K_BT)$. Then, the conductivity is predicted to note a law of the design.

$$\sigma_p(F) = \sigma_0^P \exp\left(\frac{eFs}{2K_B T}\right). \tag{18}$$

Perfectors might exhibit a susceptible discipline dependence ~Fl, where γ contrasts continuously between -2 and 0. Flexibility is roughly involved in this discipline dependence. Most of the research focuses on the sector dependence of conductivity in surface extruded materials, emphasizing small etched layers and Poole-Frenkel transport in large fields. Elmina and Zhang initially investigated the device in nanoscale PCM gadgets. In low areas, ohmic bodies were observed, while Poole-like lines were found in higher fields, which led to a reexamination of Hill's double-middle Coulomb capability version for step-extruded materials. Fermi electricity most likely brought it to the edge of the band, and it journeyed a long way inside the band before it was regained. As a result, it results in an incorrect dependency in the current due to the implemented restriction voltage. No matter what, early perceptions of the current time and the future have genuinely confirmed the existence of 3 frames. In addition, the area in which this modification occurs can vary after essential relaxation. Before that, Frenkel's pressure had been examined within the preferred environment of messy substances—Poole to Poole. In total, Figure 15 illustrates the assessment of the blocking off towards the implemented voltage of a PCM factor at special temperatures near an interruption that complies with the version. As a result, assisted tunnels and direct tunnels can be built via the border.

Among higher fields, direct degradation by the obstacle is more likely than thermal degradation, and the field dependence of conductivity follows the Fowler-Northeim-Exp equation. The Wentzel-Kramer Brillouin (WKB) can be used to calculate the probability of a total discharge through thermally assisted excavation and direct excavation of a solitary deformity. In contrast, if you shout the buzzword semiconductor, where ballistic vehicles may be found in deeply scaled devices, in undefined semiconductors, one can rely on diffuse (nonballistic) transport all the way down to the smallest dimensions of the device.

4.2. Confrontation Flow. The low-discipline resistance of PCM follows a time relationship defined by equation (19) at steady ambient temperature.

$$R(t) = R(t_0)\frac{t}{t_0}^{\nu R}. \tag{19}$$

$R(t_0)$ is the predicted impediment at the time t_0 in equation (19). $t^{\nu R}$ is glide type, which usually has a price of 0.1 for the RESET state, showing the importance between the device and the intragender version. The counterrotating glide is caused by the step extrude material. Thereby, the glide is much less for the SET state (yet; 0.05), wherein the material is predominantly inside the glassy state but rarely zero in dissolved, extinct PCM drops (Figure 14(b)). As a result of the inconsistency of diverse obstruction states and devices, PCM has the greatest potential. We present a portrait of the number one method for dealing with degree extruded materials, which is widely spread due to the propulsion of the impediment device. Lastly, we demonstrate and render the clogging glide in PCM gadgets.

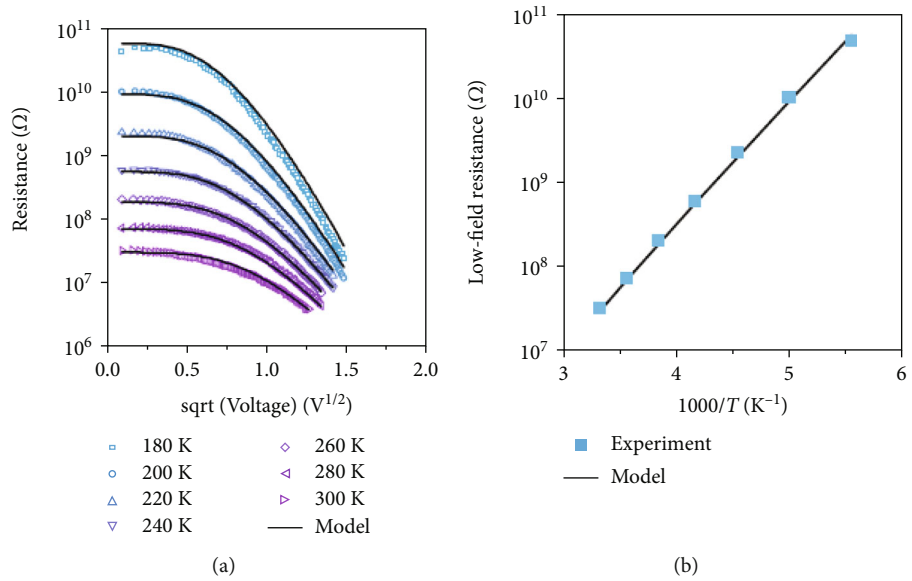

Figure 15: (a) The resistance of PCM devices within the RESET kingdom is a function of voltage at special ambient temperatures. After a RESET and heating at room temperature, the device was measured. (b) Discipline resistance. The device's R as a temperature characteristic R exhibits Arrhenius-type equation behaviour (6).

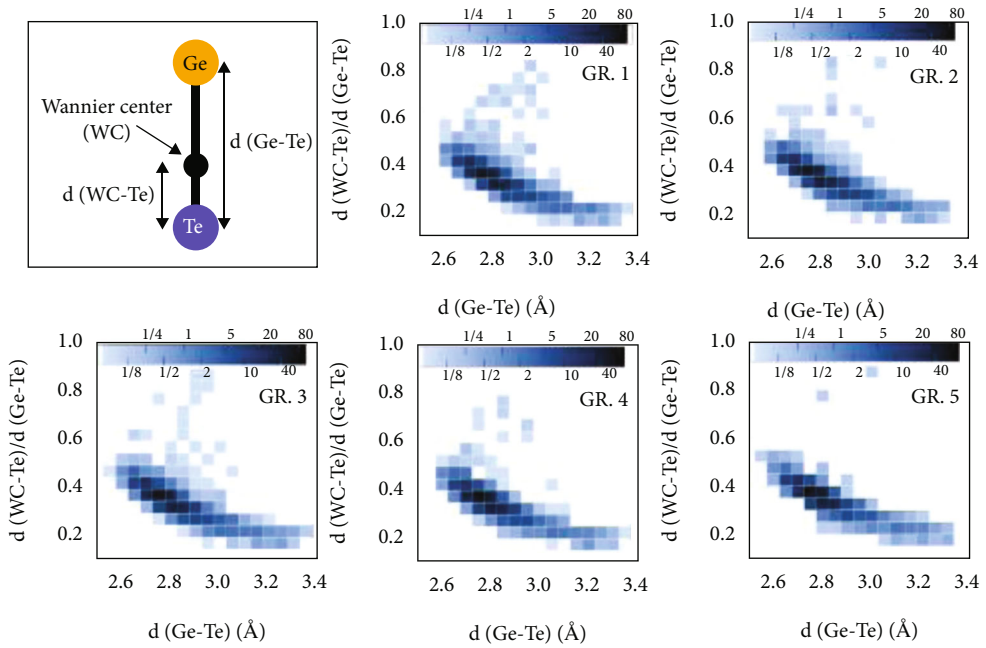

Figure 16: Bond polarizations.

4.2.1. Minuscule Origin of Fighting Drift. As a result of the unrestricted underlying processing of the reportable stage change material, floating obstructions in PCM devices have been eliminated. The primary unwind is a direct result of the amorphization cycle shown in segment 3.

Figure 16 shows bond polarizations instead of bond distances which are shown on graphs. Sixty-five structures were obtained through conventional simulations and tested using first requirements estimations. They are divided into five groups (GR) spanning 1 (better conductivity). During the glasslike stage, growth in competition is driven mainly by the development of those imperfections grouped by a slow improvement of community bonds closer to the translucent stage systems with compound request and coordination numbers. A possible evaluation at the end of those works is whether the increment in obstruction requires a shift of the Fermi stage closer to midhollow. In addition, the bandgap remains constant or increases upon switching. After shifting from GR.1 to GR.5 (parent 15), the bandgap remains impressively consistent, but they describe a reduction in the number

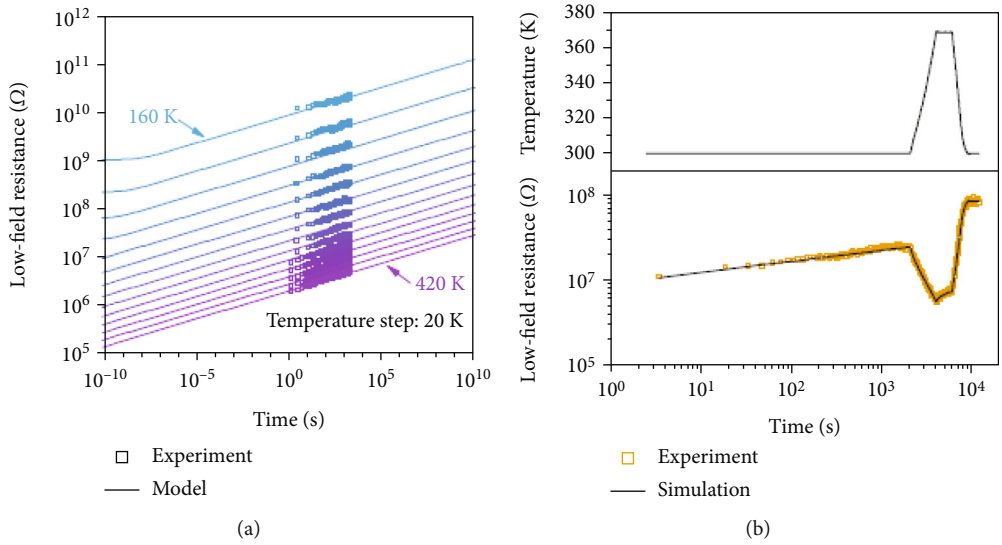

Figure 17: (a) Low-area resistance follows the flow of a PCM tool in the RESET nation at various room temperatures. (b) Low-area resistance is governed by the operation of a PCM tool within the RESET nation (bottom) and the utility of a time-variable temperature profile (top).

of states inside the bandgap, which shifts the Fermi stage closer to the midhollow. A shift of the Fermi stage adds to the actuation strength for conduction and, along with those traces, brings about an accelerated obstruction.

The other group of authors claim that bandgap broadening occurs when a shift can come about because of the enhancing mint of Peiperl's mutilation associated with a lower inside the number of tetrahedrally prepared Ge iotas. Additionally, the idea of bandgaps on the shift is examined using Fourier Extruded Infrared Spectroscopy (FTIR). The bandgap can be identified by examining the replica strategies utilized in the numerous features and the requirements used to represent the bandgap top to bottom.

4.2.2. Modeling and Classification of Flow. It is based on Gibbs' well-known unwinding model. Accordingly, most studies expected that adjusting the buoyancy resistance would be achieved by adjusting the actuation energy for the line E_a (equation (20)). Using half-hole dropouts and a widening bandgap due to a near rearrangement, it is not difficult to show that E_a has the structure.

$$E_a(t) = E_a(t_0) + E_D \log\left(\frac{t}{t_0}\right). \tag{20}$$

Based on the time-temperature overlay E_a, E_D corresponds to the temperature at which the T_{ann} detail is amplified. (t) are truly derived from the number one settlement. So we can position $E_D = \arctan$ together, explaining condition (10), while the opposing current is visualized on Cosell temperature $T = T_{\text{ann}}$. This specific dependence $E_a(t_0)$, based on condition (11) in space and time, has been provided with a provisional demonstration by several different fits with PCM. There is another dependence on the conductivity perfector t_0 of condition (6) at the scheme for positive materials, e.g., AIST, which needs similar investigations. Despite this, there is the need to show the dependence on E_a at the glide, where the boundaries represent the unwinding pattern of the material. Y is the quantity of noncomfortable deformities' part of the aggregated unwinding model. Within the aggregated unwinding version, it represents the distance between the inconvenient state and the "perfect glass" state. These strategies are both dependent on E_a. Figure 17 shows this.

The slope of $\log(I)$ compared to V within the IV mark is expected to increase with the flow. The hardening of the imperfections was demonstrated by growing the focal distance within the Poole-Frenkel version with floating. A second important limit price that adjusts while floating is the limited voltage, which is shown to rise without delay in response $\log(t/t_0)$. A variable E_a can be modified to delete the go with the flow. This has been cleverly demonstrated to increase with number one unwinding, slowing down the pace of gem development from the segment alternate material flow to save data on a PCM device. It is possible to use the nonlinearity of the casual region's IV characteristic (Figure 14(a)) to take a greater share of the state of affairs configuration discussion. It is invariant to estimate the obstruction inside of the excessive subject machine. The steepness of $\log(I)$ versus V inside the huge V, as illustrated in Figure 14(a), may be utilized to calculate the scale of the casual location. In assessment to that, it relies upon simplest at the go with the flow obstruction of the decrease subject. The most effective method to determine the overextended subject machine of any customized situation is to use an understanding of the converting voltage, which can be derived from the adjusted expression. It is then possible to locate the voltage at which a positive limit is reached. Time estimate (usually called metric) is based on the ratio of changing regions. The point of this is to make certainly

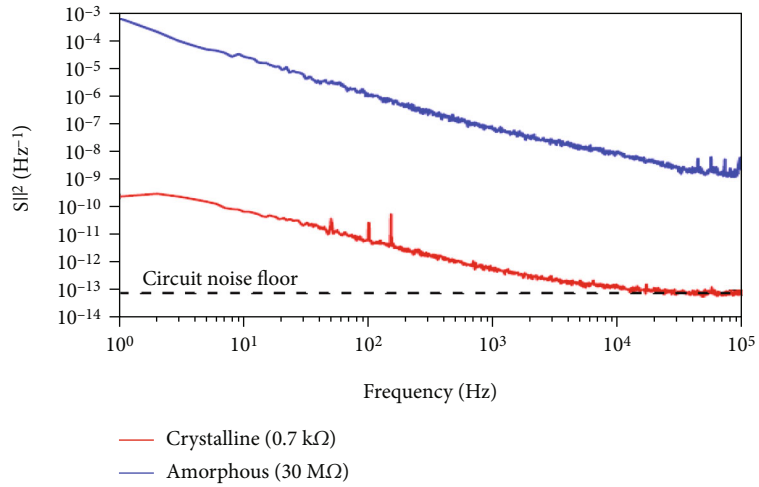

Figure 18: The amorphous and crystalline states' spectral density SI/I2 in a nanoscale Get line cell is normalized. In the tool, the applied voltage is 49 mV.

viable thinking about the profoundly nonlinear nature of the electric device on the shapeless level. In WRITE, the current movement is through the level alternative component since there is less competition of the vague on region than the obstruction of the projection fragment. However, while studying, the projection component facilitated the current movements because it has lower competition than the amorphous dispersal of the off region. Accordingly, statistics restoration and statistics stockpiling are decoupled. There are a number of bothersome properties of the undefined level, such as obstruction flow, temperature reliance, and interference, which are hidden upon study. With the aid of correct sized layers and taking out the READ current movement and temperature dependence, this technique has been shown to reduce the flow form. As a related method, a PCM system may be assembled by substituting layers of level alternate nanolayers and repression nanolayers, which have been extended, displayed to minimize noise and go with the flow while preserving different capabilities.

4.3. Noise. PCM's most noticeable disturbance is called $1/f$ commotion (or flash noise), a type of disturbance seen in electronic devices. The $1/f$ commotion is bacterized by an unearthly force that corresponds to the recurrence of the sign. In the first estimate of $1/f$ commotion in nanoscale PCM, the current ghostly thickness SI/I2 of the nebulous state was two significant degrees higher than the glasslike state. Figure 18 shows the amorphous and crystalline states' spectral density.

Further estimates in GST confirmed that SI/I2 stays reel-successfully steady concerning the carried-out voltage for sufficient low voltages. Spectra of SI/I2 for cry's slogan and undefined states predicted by nanoscale Get line cells are shown in parent 17. From 1 Hz to 100 kHz, there is a $1/f$ recurrence dependence for the vague kingdom, and SI/I2 is more than one instance higher than for the glasslike domain. It has been observed that the share of SI/I2 among nebulous and translucent states is equal to the share of competition between the two states. In addition to $1/f$ commotion, abnormal message noise can also be observed in PCM transitional obstruction states. Innovation makes swift advances in ranges that are aimed aimlessly.

Additionally, the vacillation sufficiency is significant, often resulting in larger surface pores and escapes than the newest effects and signs of the RESET kingdom. $1/f$ commotion in PCM has not been clarified by installing a unique version. Several fashions have been proposed, based on double suitable possibilities wherein both debris and electrons transfer among power minima remoted by a capacity limit W, group score variances. Showing up at a spec-trump $S(f)$, $1/f$ is usually accomplished by assuming that there are a few alternate occasions, each with a delay of $\tau = \tau 0 \exp(W/Kbi)$, where $\tau 0 - 1$ is the enterprise occurrence to surpass the limitation W. In case W is circulated consistently, this methodology yields a $1/f$ range. As a result, a framework with close stable configurations with a huge number of unwinding instances could exhibit $1/f$ commotion. There could be a source of $1/f$ commotion within the mass electric competition in fee transporter portability or attention variances due to advances within the DWP.

5. Conclusion

PCM has to be the most sophisticated resistive memory technology currently available. The material has been widely discussed and made generally available in mass. As an example, its exceptional capacity, fast read/write inactivity, high cyclical endurance, and remarkable adaptability make it an ideal competitor for applications in intelligent processing standards. In PCM, the main topics discussed are crystallization mechanism, electric vehicles, and handling bumps and shocks. Furthermore, there are also special issues relating to the PCM build cycle for additional scaling and connecting

with state-of-the-art CMOS innovation centers. The poor heating rate of pure PCMs, which reduces the energy capacity, is a significant threat to the broad deployment of PCM energy. Nanoparticles have lately gained interest in improving PCM heat conductivity while retaining higher storage capacity or charging/discharging cycles. Nanoparticles increase PCM thermal performance by distributing particles, enabling a greater charging rate. Consequently, nanomaterials accelerate the phase transition procedure. Gem development models still do not provide a precise guarantee of the last temperature change from the burning state of softening. This would help us understand the state (glass or supercooling liquid) in which gem development generally occurs at low temperatures (yet; 500 K). The exact nucleation work is not as intense as for gem development for PCM. In tight amorphous designs, it may be vital to solidify undepictable spots using low-power beats. With low-power cycles, the PCM temperature diffuses and can withstand nucleation in the focal point of a shapeless place. An option would be to create devices with special heat conditions to exchange the robust thermal resistance and capacitance, which must efficiently handle the thermal cycles needed for replacement. The majority of this material came from the first unwinding of the nebulous level alternate material. The information has been validated by using a variety of check cash and replicas of subatomic particles. This paper provides an outline of current knowledge of PCM device physics, which underpins perusing and composition activities. Consequently, we offered novel PCM devices and materials. Therefore, the total study is qualitative, and no machine learning approach is used. Because of this, we cannot say that the data is quantitative. Our work includes both test representations of the unique features found in nanoscale PCM devices and material science demonstrations. Finally, we offer our perspective on some remaining unanswered questions and suggest future exploration directions.

Data Availability

The data is available on request to corresponding author.

Conflicts of Interest

The authors have no conflict of interests regarding this article.

References

[1] L. Corey, J. R. Macola, A. S. Fauci, and F. S. Collins, "A strategic approach to COVID-19 vaccine R&D," *Science*, vol. 368, no. 6494, pp. 948–950, 2020.

[2] M. Le Gallo and A. Sebastian, "An overview of phase-change memory device physics," *Journal of Physics D: Applied Physics*, vol. 53, no. 21, article 213002, 2020.

[3] S. Sivananthan, K. Ravi, and C. S. J. Samuel, "Effect of SiC particles reinforcement on mechanical properties of aluminium 6061 alloy processed using stir casting route," *Materials Today: Proceedings*, vol. 21, pp. 968–970, 2020.

[4] K. Jairath, N. Singh, M. Shabaz, V. Jagota, and B. K. Singh, "Performance analysis of metamaterial-inspired structure loaded antennas for harrow range wireless communication," *Scientific Programming*, vol. 2022, Article ID 7940319, 17 pages, 2022.

[5] J. J. M. Hillary, R. Ramamoorthi, J. D. J. Joseph, and C. S. J. Samuel, "A study on microstructural effect and mechanical behaviour of Al6061–5%SiC–TiB_2particulates reinforced hybrid metal matrix composites," *Journal of Composite Materials*, vol. 54, no. 17, pp. 2327–2337, 2020.

[6] S. O. Mezan, S. M. Absi, A. H. Jabbar, M. S. Roshan, and M. A. Agam, "Synthesis and characterization of enhanced silica nanoparticle (SiO_2) prepared from rice husk ash immobilized of 3-(chloropropyl) triethoxysilanea," *Materials Today: Proceedings*, vol. 42, Part 5, pp. 2464–2468, 2021.

[7] P. Gupta, P. Lohia, and D. K. Dwivedi, "Phase change memory: operation, current challenges and future prospects," *International Journal of Engineering, Science and Technology*, vol. 13, no. 1, pp. 93–97, 2021.

[8] S. K. Shah, F. G. Miller, T. C. Darton et al., "Ethics of controlled human infection to address COVID-19," *Science*, vol. 368, no. 6493, pp. 832–834, 2020.

[9] V. Jagota and R. K. Sharma, "Wear volume prediction of AISI H13 die steel using response surface methodology and artificial neural network," *Journal of Mechanical Engineering and Sciences*, vol. 14, no. 2, pp. 6789–6800, 2020.

[10] S. J. S. Chelladurai, S. S. Kumar, N. Venugopal, A. P. Ray, T. C. Manjunath, and S. Gnanasekaran, "A review on mechanical properties and wear behaviour of aluminium based metal matrix composites," *Materials Today: Proceedings*, vol. 37, pp. 908–916, 2021.

[11] N. Verma, V. Jagota, A. C. Alguno, M. R. Alimuddin, P. Kumar, and B. N. Dugbakie, "Characterization of fabricated gold-doped ZnO nanospheres and their use as a photocatalyst in the degradation of DR-31 dye," *Journal of Nanomaterials*, vol. 2022, Article ID 7532332, 8 pages, 2022.

[12] G. Murugesan, T. I. Ahmed, J. Bhola et al., "Fuzzy logic-based systems for the diagnosis of chronic kidney disease," *BioMed Research International*, vol. 2022, Article ID 2653665, 15 pages, 2022.

[13] S. K. Karm, "Impact of COVID-19 on Nepalese economy," *International Journal of Social Sciences*, vol. 8, no. 2, pp. 348–351, 2021.

[14] B. S. Graham, "Rapid COVID-19 vaccine development," *Science*, vol. 368, no. 6494, pp. 945-946, 2020.

[15] A. M. Khaleghi, D. Xu, Z. Wang et al., "A DDDAMS-based planning and control framework for surveillance and crowd control via UAVs and UGVs," *Expert Systems with Applications*, vol. 40, no. 18, pp. 7168–7183, 2013.

[16] M. Pérez-Ortiz, J. M. Peña, P. A. Gutiérrez, J. Torres-Sánchez, C. Hervas-Martínez, and F. López-Granados, "A semi-supervised system for weed mapping in sunflower crops using unmanned aerial vehicles and a crop row detection method," *Applied Soft Computing*, vol. 37, pp. 533–544, 2015.

[17] M. K. Loganathan, B. Mishra, C. M. Tan, T. Kongsvik, and R. N. Rai, "Multi-criteria decision making (MCDM) for the selection of Li-ion batteries used in electric vehicles (EVs)," *Materials Today: Proceedings.*, vol. 41, pp. 1073–1077, 2021.

[18] A. Kumar, V. Jagota, R. Q. Shawl et al., "Wire EDM process parameter optimization for D2 steel," *Materials Today: Proceedings*, vol. 37, no. 2, pp. 2478–2482, 2021.

[19] V. Jagota and R. K. Sharma, "Interpreting H13 steel wear behavior for austenitizing temperature, tempering time and

temperature," *Journal of the Brazilian Society of Mechanical Sciences and Engineering*, vol. 40, no. 4, pp. 1–12, 2018.

[20] G. Murugesan, T. I. Ahmed, M. Shabaz et al., "Assessment of mental workload by visual motor activity among control group and patient suffering from depressive disorder," *Computational Intelligence and Neuroscience*, vol. 2022, Article ID 8555489, 10 pages, 2022.

[21] H. Ali, H. Babar, T. Shah, M. Sajid, M. Qasim, and S. Javed, "Preparation techniques of TiO_2 nanofluids and challenges: a review," *Applied Sciences*, vol. 8, no. 4, p. 587, 2018.

[22] Y. Hwang, J. K. Lee, C. H. Lee et al., "Stability and thermal conductivity characteristics of nanofluids," *Thermochimica Acta*, vol. 455, no. 1–2, pp. 70–74, 2007.

[23] S. T. Latibari, M. Mehrali, M. Mehrali, T. M. I. Mahlia, and H. S. C. Metselaar, "Synthesis, characterization and thermal properties of nanoencapsulated phase change materials via sol-gel method," *Energy*, vol. 61, pp. 664–672, 2013.

[24] S. Harikrishnan, M. Deenadhayalan, and S. Kalaiselvam, "Experimental investigation of solidification and melting characteristics of composite PCMs for building heating application," *Energy Conversion and Management*, vol. 86, pp. 864–872, 2014.

[25] F. Bahiraei, A. Fartaj, and G.-A. Nazri, "Experimental and numerical investigation on the performance of carbon-based nanoenhanced phase change materials for thermal management applications," *Energy Conversion and Management*, vol. 153, pp. 115–128, 2017.

[26] R. Parameshwaran, K. Deepak, R. Saravanan, and S. Kalaiselvam, "Preparation, thermal and rheological properties of hybrid nanocomposite phase change material for thermal energy storage," *Applied Energy*, vol. 115, pp. 320–330, 2014.

[27] C. G. Sorensen, L. Pesonen, S. Fountas et al., "A user-centric approach for information modelling in arable farming," *Computers and Electronics in Agriculture*, vol. 73, no. 1, pp. 44–55, 2010.

[28] E. R. Hunt, W. D. Hively, S. Fujikawa, D. Linden, C. S. Daughtry, and G. McCarty, "Acquisition of NIR-green-blue digital photographs from unmanned aircraft for crop monitoring," *Remote Sensing*, vol. 2, no. 1, pp. 290–305, 2010.

[29] A. Mathews and J. Jensen, "Visualizing and quantifying vineyard canopy LAI using an unmanned aerial vehicle (UAV) collected high density structure from motion point cloud," *Remote Sensing*, vol. 5, no. 5, pp. 2164–2183, 2013.

[30] Y. Lan, S. J. Thomson, Y. Huang, W. C. Hoffmann, and H. Zhang, "Current status and future directions of precision aerial application for site- specific crop management in the USA," *Computers and Electronics in Agriculture*, vol. 74, no. 1, pp. 34–38, 2010.

[31] C. Hung, Z. Xu, and S. Succories, "Feature learning based approach for weed classification using high resolution aerial images from a digital camera mounted on a UAV," *Remote Sensing*, vol. 6, no. 12, pp. 12037–12054, 2014.

[32] M. Yang, P. Kumar, J. Bhola, and M. Shabaz, "Development of image recognition software based on artificial intelligence algorithm for the efficient sorting of apple fruit," *International Journal of System Assurance Engineering and Management*, vol. 13, no. 1, pp. 322–330, 2021.

[33] S. Abusua and M. N. Jothi, "A secure colour image using integer wavelet transform with Linde-Bubo Gray algorithm," *International Research Journal of Engineering and Technology*, vol. 3, no. 4, 2014.

[34] J. Sharma and R. Thapa, "Hybrid approach for data security using RSA and LSB algorithm," *Proceedings of IOE Graduate Conference*, vol. 7, 2019.

[35] W. H. Press, *FORTRAN Numerical recipes*, Cambridge University Press, Cambridge [England]; New York, 2nd edition, 1996.

[36] D. S. Watkins, *Fundamentals of Matrix Computations*, John Wiley & Sons, 2004.

[37] M. Petrous and C. Petrous, *Image Processing: The Fundamentals*, Wiley, 1st edition, 2010.

[38] M. Guilherme, E. Glaser, and M. Mendez Garcia, "The pragmatics of intercultural competence in education and training: a cross-national experiment on 'diversity management," in *Becoming Interculturally Competent through Education and Training*, A. Feng, M. Byram, and M. Fleming, Eds., pp. 193–210, Multilingual Matters, 2009.

[39] D. M. Dekker, C. G. Rutte, and P. T. Van den Berg, "Cultural differences in the perception of critical interaction behaviors in global virtual teams," *International Journal of Intercultural Relations*, vol. 32, no. 5, pp. 441–452, 2008.

[40] S. L. Tariq, H. M. Ali, M. A. Akram, M. M. Janjua, and M. Ahmadlouydarab, "Nanoparticles enhanced phase change materials (NePCMs)-a recent review," *Applied Thermal Engineering*, vol. 176, article 115305, 2020.

[41] J. Wang, H. Xie, Z. Xin, Y. Li, and L. Chen, "Enhancing thermal conductivity of palmitic acid based phase change materials with carbon nanotubes as fillers," *Solar Energy*, vol. 84, no. 2, pp. 339–344, 2010.

[42] F. Yavari, H. Fard, K. Pashayi et al., "Enhanced thermal conductivity in a nanostructured phase change composite due to low concentration graphene additives," *Journal Physical Chemistry C*, vol. 115, no. 17, pp. 8753–8758, 2011.

[43] X. Tong, M. Zhang, L. Lei, H. Zhang, and J. Qiu, "Research on themodification of microencapsulated phase change material for thermalenergy storage by nano-SiO_2 and graphite," *New Chemical Materials (China)*, vol. 38, no. 9, pp. 128–130, 2018.

[44] Q. Song, Y. Li, J. Xing, J. Y. Hu, and Y. Marcus, "Thermal stability of composite phase change material microcapsules incorporated with silver nano-particles," *Polymer*, vol. 48, no. 11, pp. 3317–3323, 2007.

[45] M. Hums and A. H. Reilly, "Managing intercultural teams: the eorganization exercise," *Journal of Management Education*, vol. 32, no. 1, pp. 118–137, 2008.

[46] A. Martínez-Sánchez, M. Pérez-Pérez, P. de-Luis-Carnicer, and M. José Vela-Jiménez, "Teleworking and new product development," *Euro Journal of Inn Management*, vol. 9, no. 2, pp. 202–214, 2006.

[47] K. L. Gretsch, "Working with global virtual teams: a case study reality check on intercultural communication best practices," *Global Advances in Business Communication*, vol. 5, no. 1, 2016.

[48] V. O. Onodera, V. T. Emma, and O. E. Taylor, "An integrated data hiding technique using Steg-Crypto Method," *Journal of Digital Innovations & Contemporary Research in Science & Engineering*, vol. 5, no. 2, p. 13, 2017.

[49] D. B. Roebuck, S. J. Brock, and D. R. Moodie, "Using a simulation to explore the challenges of communicating in a virtual team," *Business Communication Quarterly*, vol. 67, no. 3, pp. 359–367, 2004.

[50] S. Lloyd and C. Hertel, "Intercultural competencies for culturally diverse work teams," *Journal of Managerial Psych*, vol. 25, no. 8, pp. 845–875, 2010.

[51] E. Shove, "What is wrong with energy efficiency?," *Building Research & Information*, vol. 46, no. 7, pp. 779–789, 2018.

[52] K. Gillingham, A. Keyes, and K. Palmer, "Advances in evaluating energy efficiency policies and programs," *Annual Review of Resource Economics*, vol. 10, no. 1, pp. 511–532, 2018.

[53] M. O. I. Musa, T. E. H. El-Gorshin, and J. M. H. Amirkhani, "Bounds on GreenTouch GreenMeter network energy efficiency," *Journal of Lightwave Technology*, vol. 36, no. 23, pp. 5395–5405, 2018.

[54] H. Tatiana, L. M. Karpenko, F. V. Olesya, S. I. Yu, and D. Svetlana, "Innovative methods of performance evaluation of energy efficiency Projects," *Academy of Strategic Management Journal*, vol. 17, no. 2, p. 12, 2018.

[55] E. Kavalski and S. F. Jackson, *China's Regional Relations in Comparative Perspective: From Harmonious Neighbors to Strategic Partners*, Routledge, England, UK, 2018.

[56] A. Ali, "China Pakistan economic corridor: prospects and challenges for regional integration," *Arts and Social Sciences Journal*, vol. 7, no. 4, 2016.

[57] M. Esteban, "The China-Pakistan corridor," *Strategic Studies*, vol. 36, no. 2, pp. 63–74, 2016.

[58] M. Haider and N. Hussain, "The role of Pakistan and China in Afghanistan: prospects for regional cooperation," *Pakistan Journal of History and Culture*, vol. 41, no. 1, 2020.

[59] H. A. Rizvi, "The China-Pakistan economic corridor," *Strategic Studies*, vol. 34, pp. 1–17, 2014.

[60] Z. Korzeb and P. Niedziółka, "Condition of banks listed on the Warsaw Stock Exchange during the first 3 months of the pandemic in Poland," *Journal of Banking and Financial Economics*, vol. 2, no. 14, pp. 5–20, 2020.

[61] D. Talbot and E. Ordonez-Ponce, "Canadian banks' responses to COVID-19: a strategic positioning analysis," *Journal of Sustainable Finance & Investment*, vol. 12, no. 2, pp. 423–430, 2022.

[62] D. Wojcik and S. Ioannou, "COVID-19 and finance: market developments so far and potential impacts on the financial sector and centres," *Tijdschrift Voor Economische En Sociale Geografie*, vol. 111, no. 3, pp. 387–400, 2020.

[63] A. Aguilera, Lethiais, Rallet, and Proulhac, "Home-based telework in France: characteristics, barriers and perspectives," *Transportation Research Part A: Policy and Practice*, vol. 92, pp. 1–11, 2016.

[64] A. Belzoni and A. Arrogances, "Teleworking in the context of the Covid-19 crisis," *Sustainability*, vol. 12, no. 9, p. 3662, 2020.

[65] J. Arellano, L. Márquez, and V. Cantillon, "COVID-19 outbreak in Colombia: an analysis of its impacts on transport systems," *Journal of Advanced Transportation*, vol. 2020, Article ID 8867316, 16 pages, 2020.

[66] A. G. Raisin, V. Capuano, K. Varkulevičiūtė, and K. Arachova, "Working from home—who is happy? A survey of Lithuania's employees during the COVID-19 quarantine period," *Sustainability*, vol. 12, no. 13, p. 5332, 2020.

[67] İ. Bekçi, K. Ö. Eda, and E. Aksoy, "COVID-19'un Türkiye'de bankalar üzerindeki ekonomik etkisine dair bir tahmin," *Economic, Political & Finnans Araştırmaları Derigs*, vol. 5, 2020.

[68] S. Singh and V. K. Atria, "Dual layer security of data using LSB image steganography method and AES encryption algorithm," *International Journal of Signal Processing, Image Processing and Pattern Recognition*, vol. 8, no. 5, pp. 259–266, 2015.